

Article

Half-Period Gray-Level Coding Strategy for Absolute Phase Retrieval

Zipeng Ran ^{1,2} , Bo Tao ³ , Liangcai Zeng ⁴ and Xiangcheng Chen ^{2,5,*}¹ School of Automation, Wuhan University of Technology, Wuhan 430070, China; rzp@whut.edu.cn² Key Laboratory of Icing and Anti/De-Icing, China Aerodynamics Research and Development Center, Mianyang 621000, China³ Hubei Key Laboratory of Mechanical Transmission and Manufacturing Engineering, Wuhan University of Science and Technology, Wuhan 430081, China; taoboq@wust.edu.cn⁴ Key Laboratory of Metallurgical Equipment and Control Technology of Ministry of Education, Wuhan University of Science and Technology, Wuhan 430081, China; zengliangcai@wust.edu.cn⁵ School of Artificial Intelligence, Anhui University, Hefei 230039, China

* Correspondence: chenxgcg@ustc.edu

Abstract: N-ary gray-level (nGL) coding strategy is an effective method for absolute phase retrieval in the fringe projection technique. However, the conventional nGL method contains many unwrapping errors at the boundaries of codewords. In addition, the number of codewords is limited in only one pattern. Consequently, this paper proposes a new gray-level coding method based on half-period coding, which can improve both these two deficiencies. Specifically, we embed every period with a 2-bit codeword, instead of a 1-bit codeword. Then, special correction and decoding methods are proposed to correct the codewords and calculate the fringe orders, respectively. The proposed method can generate n^2 codewords with n gray levels in one pattern. Moreover, this method is insensitive to moderate image blurring. Various experiments demonstrate the robustness and effectiveness of the proposed strategy.

Keywords: fringe projection; absolute phase retrieval; gray-level coding; half-period coding



Citation: Ran, Z.; Tao, B.; Zeng, L.; Chen, X. Half-Period Gray-Level Coding Strategy for Absolute Phase Retrieval. *Photonics* **2022**, *9*, 492. <https://doi.org/10.3390/photonics9070492>

Received: 4 May 2022

Accepted: 11 July 2022

Published: 14 July 2022

Publisher's Note: MDPI stays neutral with regard to jurisdictional claims in published maps and institutional affiliations.



Copyright: © 2022 by the authors. Licensee MDPI, Basel, Switzerland. This article is an open access article distributed under the terms and conditions of the Creative Commons Attribution (CC BY) license (<https://creativecommons.org/licenses/by/4.0/>).

1. Introduction

Optical three-dimensional (3D) measurement technology is now a hot research topic in many fields such as industrial inspection, biomedicine, virtual reality and reverse engineering [1–3]. Among various optical methods, digital fringe projection (DFP) is widely used for its characteristics of high speed, high accuracy and easy set-up [4–8]. In a typical DFP system, a projector projects some predesigned fringe patterns onto the measured object, and a camera is used to capture the deformed patterns modulated by the object's profile. Then, a suitable digital fringe analysis method is selected to calculate the phase map which reveals the relationship between the depth and the distribution of the object's surface. After system calibration [9–11], the real 3D world coordinates of the object surface can be recovered based on the phase map.

Many digital fringe analysis methods have been developed for phase retrieval, among which Fourier transform profilometry (FTP) [12–14] and phase shifting profilometry (PSP) [15–18] are the most widely used. FTP is suitable for dynamic measurement because it only projects one single-shot pattern, so the speed can be as fast as the camera frame rate. However, the accuracy of FTP will drop sharply when facing complex surfaces with abrupt changes. In contrast to FTP, PSP, which requires more than one pattern (normally at least three) to reconstruct the 3D shape of the object, has high accuracy at the cost of speed. As a result, it is often applied for static and low-speed measurement. Unfortunately, due to the use of arctangent function, the phase map recovered by both FTP and PSP ranges from 0 to 2π with 2π discontinuities, known as the wrapped phase. Furthermore, phase

discontinuities turn the originally continuous absolute phase into the range of $[0, 2\pi]$. After each cycle, the phase value decreases by 2π . In other words, the wrapped phase loses the information of fringe order k of every cycle. Therefore, phase unwrapping techniques are necessary to calculate the fringe order k and then recover the absolute phase.

The existing phase unwrapping algorithms can be classified into two principle categories: spatial algorithms and temporal algorithms [7]. Spatial algorithms such as reliability-guided [19] and quality-guided methods [20,21] tend to fail when dealing with large discontinuities and isolated objects. Unlike spatial algorithms, temporal algorithms project extra patterns to provide additional information on the fringe order; thus, the accuracy of temporal methods is much higher than spatial methods. Currently, popular temporal unwrapping methods include two-wavelength [22,23], multiple-wavelength [24], gray-code [25,26] and phase-coding methods [27–29]. Among them, the gray-code method which encodes patterns with binary intensity values has a wide range of application for its easy-to-understand principles and robustness. Yet, only two intensities being employed limit the number of codewords. Concretely, m patterns can only generate 2^m codewords. In order to expand the amount of codewords, the n -ary gray-level (nGL) method [30–36] that uses $n > 2$ intensity values was developed. In the nGL method, the number can be broadened to n^m with the same m patterns.

However, in real measurement, it is likely that some of the codewords at the 2π boundaries would be calculated inaccurately and would thus lead to unwrapping errors, which has become a major challenge to be solved in gray-level methods. Many methods were proposed to improve this deficiency. Chen et al. [31] modified the sequences of the nGL method's codewords in a way that is similar to gray-code. Specifically, two neighboring codewords are arranged to differ only by one gray-level, so that the boundary unwrapping errors can be removed in principle. Zheng [26] improved this deficiency of the gray-code method when measuring step-heights, based on an adaptive median filter. Wu [34] proposed a shifting gray-code method to eliminate boundary errors in the defocused scene. Cai et al. [32] proposed a half-period correction method which can correct wrong boundary codewords in both noisy and defocused situations. In this method, two half-period masks are generated combining the wrapped phase. Then, each mask can be utilized to align and correct halves of the codewords. However, this method still requires the projection of six fringe patterns, which is too many for high-speed measurement. Inspired by Cai's method, we propose a new gray-level coding method based on half-period coding. Specifically, Cai uses two half-period masks to divide a 1-bit codeword into two halves for alignment and correction, but the code of each half is actually the same. Yet, we consider that each half might not always have to be the same. In fact, each half-period mask can be utilized to determine its own half-code. Therefore, we embed every half-period with a code, so that each period is assigned with a 2-bit codeword, thus generating more codewords in one pattern. The proposed unwrapping method guarantees more robust unwrapping results. In addition, the proposed method requires the projection of only one additional pattern to unwrap the wrapped phase when compared to other temporal unwrapping methods, which has the potential to be applied in high-speed measurement.

The remainder of the paper is organized as follows: Section 2 presents the principles of the proposed method in detail; Section 3 demonstrates the robustness of our method with experiments; Section 4 summarizes the whole paper.

2. Principles

2.1. Three-Step Phase-Shifting Method

PSP is one of the most widely used methods in fringe projection for phase recovery due to its high accuracy and fast speed. Among various PSP algorithms, the three-step phase-shifting method requires the least number of patterns, thus becoming the best choice in

high-speed measurement. Three sinusoidal phase-shift patterns with $2\pi/3$ shifts captured by camera can be mathematically described as:

$$I_1(x, y) = A(x, y) + B(x, y) \cos[\varphi(x, y) - \frac{2\pi}{3}], \tag{1}$$

$$I_2(x, y) = A(x, y) + B(x, y) \cos[\varphi(x, y)], \tag{2}$$

$$I_3(x, y) = A(x, y) + B(x, y) \cos[\varphi(x, y) + \frac{2\pi}{3}], \tag{3}$$

where $A(x,y)$ denotes the average intensity of the image, $B(x,y)$ represents the fringe contrast or the so-called intensity modulation, and $\varphi(x,y)$ is the wrapped phase waiting to be solved. Combining Equations (1)–(3), the three variables mentioned above can be calculated as:

$$A(x, y) = \frac{I_1 + I_2 + I_3}{3}, \tag{4}$$

$$B(x, y) = \frac{1}{3} \sqrt{3(I_1 - I_3)^2 + (2I_2 - I_1 - I_3)^2}, \tag{5}$$

$$\varphi(x, y) = \tan^{-1} \left(\sqrt{3} \frac{I_1 - I_3}{2I_2 - I_1 - I_3} \right), \tag{6}$$

A and B can be utilized to generate a mask which can remove the background, according to a suitable threshold. The mask can be calculated by:

$$Mask = \begin{cases} 1, & \text{if } (B/A) > \text{threshold} \\ 0, & \text{otherwise} \end{cases}. \tag{7}$$

Due to the use of arctangent function from Equation (6), the wrapped phase will be limited in the range of $[0, 2\pi]$ with 2π jumps. In order to gain the absolute phase, phase unwrapping must be applied to remove these discontinuities. Once the fringe order is determined by the appropriate unwrapping method, the absolute phase can be solved by:

$$\Phi(x, y) = \varphi(x, y) + 2\pi \times k(x, y), \tag{8}$$

where $\Phi(x,y)$ is the absolute phase and $k(x,y)$ is the fringe order calculated by the phase unwrapping method.

2.2. The Proposed Method

2.2.1. Coding Strategy

The proposed method encodes every half-period with a code, so each period has a 2-bit codeword. In general, n intensity levels are able to generate n^2 different codewords. Without loss of generality, this paper selects $n = 4$ intensity levels, generating 16 fringe orders. The specific codewords for each period are listed in Table 1. C_1 cycles in the loop of ‘1234’ four times and C_2 is arranged as ‘1234234134124123’. C_1 and C_2 can form a unique 2-bit codeword C_1C_2 together to determine the fringe order. Figure 1 shows the designed codewords, where C_1 and C_2 are plotted in green and red, respectively. From this picture, we can see that every period is embedded with a 2-bit codeword. Let C_1 and C_2 be the sequences shown in Table 1. Then, the codes can be mathematically described as:

$$code = \begin{cases} C_1, & \text{if } 0 < \text{mod}(x, P) \leq \frac{P}{2} \\ C_2, & \text{if } \frac{P}{2} < \text{mod}(x, P) \leq P \end{cases} \tag{9}$$

where x represents the horizontal location of the pattern and P denotes the number of pixels per period. If x lies in the first half-period, code is assigned to C_1 . In contrast, if x lies in

the second half-period, code is assigned to C_2 . Consequently, the coded pattern can be described by:

$$I_1(x,y) = A(x,y) + B(x,y) \times \left(\frac{2code - 5}{3}\right), \tag{10}$$

where $A(x,y)$ and $B(x,y)$ are the average intensity and intensity modulation, respectively. Generally, both $A(x,y)$ and $B(x,y)$ are set to 0.5 to generate four gray levels of $\{0, 1/3, 2/3, 1\}$.

Table 1. The designed codewords of the proposed method.

k	1	2	3	4	5	6	7	8	9	10	11	12	13	14	15	16
C_1	1	2	3	4	1	2	3	4	1	2	3	4	1	2	3	4
C_2	1	2	3	4	2	3	4	1	3	4	1	2	4	1	2	3
C_1C_2	11	22	33	44	12	23	34	41	13	24	31	42	14	21	32	43

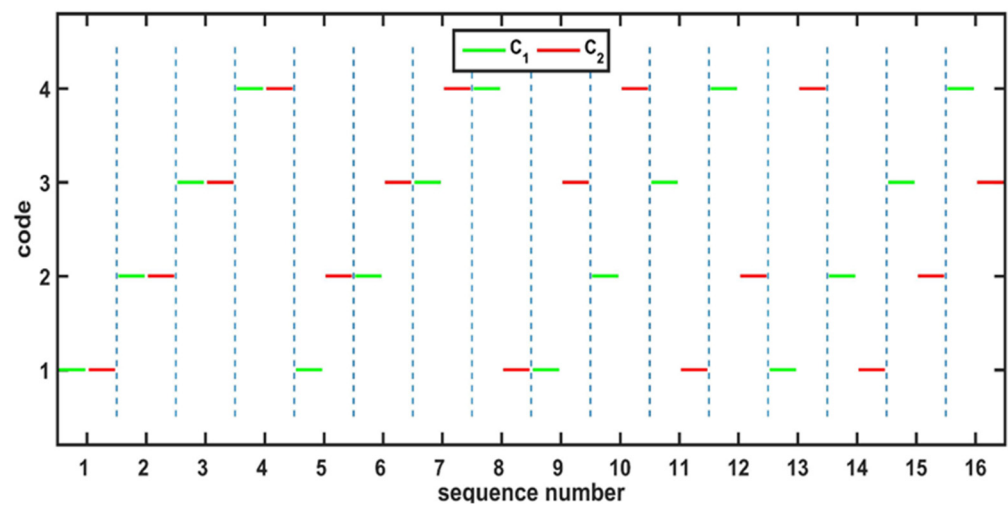


Figure 1. The designed codewords of the proposed method.

The four fringe patterns to be projected are presented in Figure 2. Figure 2a shows the three sinusoidal patterns, which are used to obtain the wrapped phase. Figure 2b displays the pattern of the proposed method, which is employed to compute the fringe order.

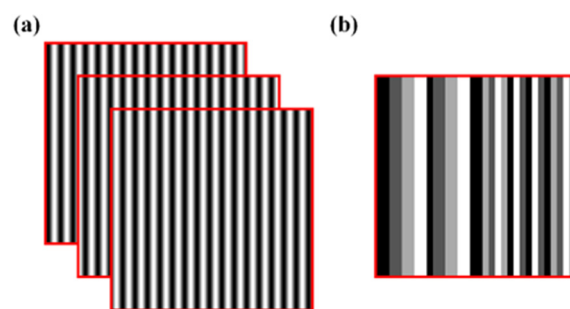


Figure 2. Patterns used in the proposed method. (a) Three sinusoidal patterns. (b) The coded pattern.

2.2.2. Unwrapping Strategy

The procedure of the unwrapping strategy is presented in Figure 3, and the detailed steps of the method are described as follows:

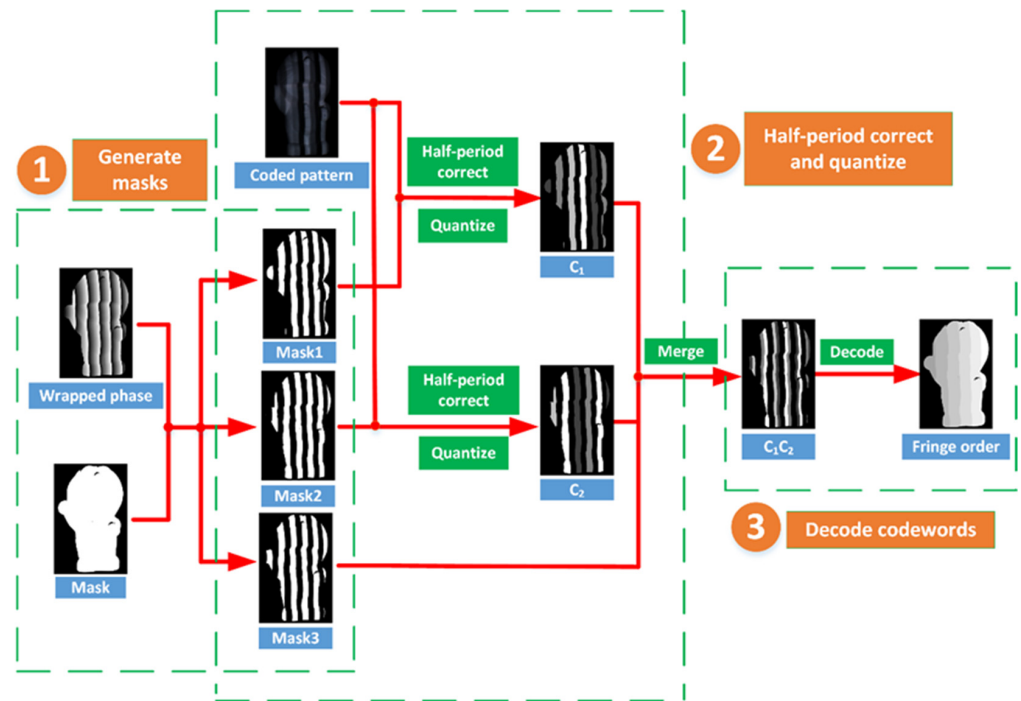


Figure 3. The procedure of the unwrapping strategy.

Step 1: Generate masks. As Equations (6) and (7) indicate, we can obtain the wrapped phase $\phi(x, y)$ and *Mask* to remove the background. Afterwards, three masks can be produced by the wrapped phase $\phi(x, y)$ and *Mask*. The process is shown in Figure 3 and the three masks can be mathematically presented by:

$$Mask1 = \begin{cases} 1, & \text{if } 0 < \phi(x, y) \leq \pi \\ 0, & \text{if } \pi < \phi(x, y) \leq 2\pi' \end{cases} \quad (11)$$

$$Mask2 = \begin{cases} 0, & \text{if } 0 < \phi(x, y) \leq \pi \\ 1, & \text{if } \pi < \phi(x, y) \leq 2\pi' \end{cases} \quad (12)$$

$$Mask3 = \begin{cases} 1, & \text{if } \pi/2 < \phi(x, y) \leq 3\pi/2 \\ 0, & \text{otherwise} \end{cases}, \quad (13)$$

Mask1 and *Mask2* are used to correct and quantize C_1 and C_2 , while *Mask3* is used to merge them into a 2-bit codeword C_1C_2 .

Step 2: Correct and quantize half-period. Due to sharp changes between the intensities of C_1 and C_2 , some of the boundary pixels would be calculated inaccurately. For example, the codeword of the 13th period is assigned as ‘14’, but in practice some pixels in the boundary of C_1 and C_2 might be computed as ‘2’ or ‘3’. Different from Cai’s method that corrects two identical parts of a 1-bit codeword, the half-period correction method is applied to correct two different bits of a 2-bit codeword. In detail, we first multiply the captured coded pattern with *Mask1* and *Mask2* to align the maps of C_1 and C_2 with the wrapped phase at every 2π boundary. Then, we use a *bwlabel* function in Matlab to segment and mark the connected regions. After that, we compute the average intensity value of every labeled region and replace each region with the average value. Thus, the wrong boundary codewords can be corrected. Briefly, this correction method makes use of characteristics of the wrapped phase to align the codewords at each 2π boundary, and then employs an averaging operation to reduce the errors brought about by noises and reduce defocusing to the least level. As a result, it can eliminate the errors at the boundaries to a great extent.

After correcting, we quantize these regions into four gray levels {1, 2, 3, 4} according to their mean values by suitable thresholds. In this way, we obtain the corrected and quantized maps of C_1 and C_2 . Next, we use an AND function among the two maps and $Mask_3$. Then, we can acquire the map of 2-bit codewords C_1C_2 . It is clear to see in Figure 3 that this map is split into many stripes and each stripe corresponds to a 2-bit codeword.

Step 3: Decode codewords. The codewords include normal codewords and defective codewords. Figure 4 gives the detailed process. The normal codewords represent those complete codewords that have both C_1 and C_2 in one period. For this kind of codeword, it is easy to find the corresponding fringe orders by the look-up table given in Table 1.

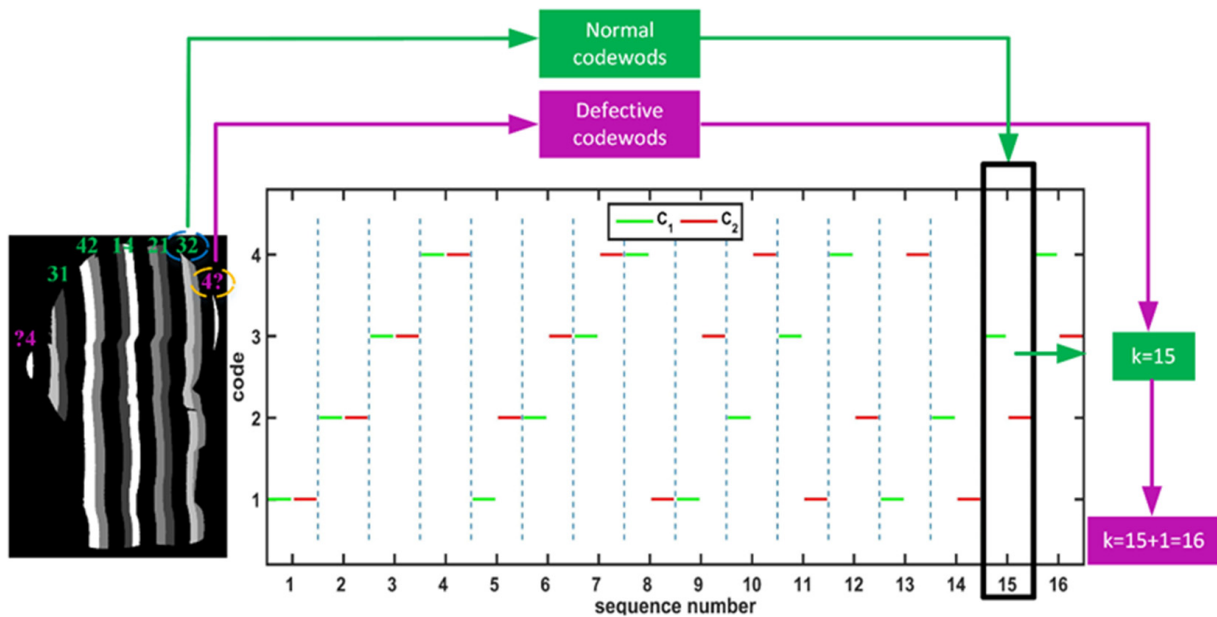


Figure 4. The process of decoding.

The defective codewords are the incomplete codewords which lose either C_1 or C_2 , due to the location of the objects or the inappropriate thresholds. These defective codewords cannot be determined directly but can be calculated by referring to their adjacent codewords. In other words, if we have calculated the fringe order of the previous codeword or the next codeword, the fringe order of the current defective codeword can be obtained by its previous fringe order plus one or the next fringe order minus one. Once all the codewords are decoded, the absolute phase can be recovered based on Equation (8).

3. Simulation

In this section, the hypothesis that the proposed coding method is able to correctly calculate the fringe order in defocused scenes was validated in simulations. In general, the image blurring can be obtained through a convolution operation with the point spread function (PSF) which can be approximated by a 2D Gaussian filter [37]:

$$G(x, y) = \frac{1}{2\pi\sigma^2} \exp\left(-\frac{x^2 + y^2}{2\sigma^2}\right), \tag{14}$$

where σ denotes the standard deviation and its value determines the degree of blurring. Therefore, different degrees of image blurring can be obtained by setting different values of σ . The 2D Gaussian filters can be easily generated by the use of the special function in Matlab. In this simulation, the period of the coded patterns was 36 pixels. Three Gaussian filters with $\sigma = 5$, $\sigma = 10$ and $\sigma = 15$ were generated, which can be seen in Figure 5a,d,g, respectively. To test the feasibility of the proposed method, the three patterns of different degrees were utilized to solve the fringe order and the absolute phase through our method.

The results are shown in Figure 5b,c, Figure 5e,f and Figure 5h,i, respectively. We can see that in the first two situations of $\sigma = 5$ and $\sigma = 10$, our method could still correctly obtain the fringe order and reconstruct the reference plane. However, in the last situation when the σ increased to 15, the image became severely blurred and our method failed. From this simulation, we can draw the conclusion that the proposed method is applicable in moderate defocused scenes. When the blurring becomes severe, the proposed method will be likely to fail.

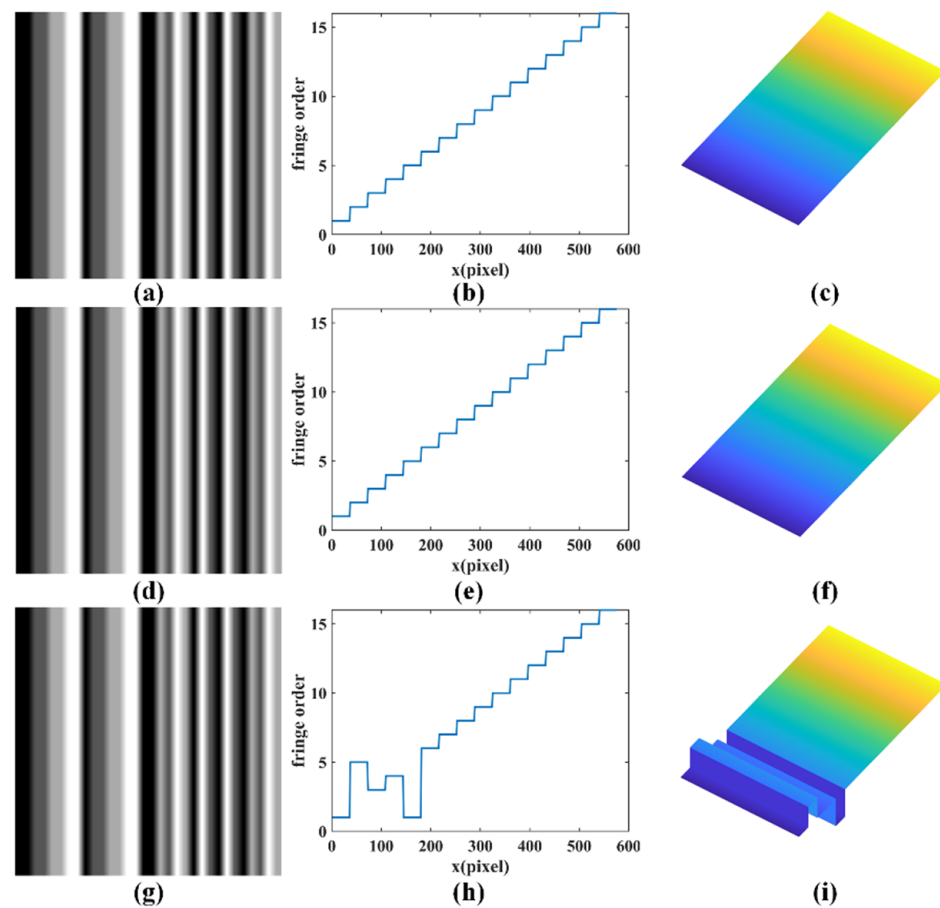


Figure 5. Blurred reference patterns and results of simulation with different standard deviation σ . (a–c) Blurred reference pattern, one section of fringe order and reconstruction of reference plane with $\sigma = 5$, respectively. (d–f) Blurred reference pattern, one section of fringe order and reconstruction of reference plane with $\sigma = 10$, respectively. (g–i) Blurred reference pattern, one section of fringe order and reconstruction of reference plane with $\sigma = 15$, respectively.

4. Experiments

To verify the performance of the proposed method, a DFP system was set up including a digital projector (LightCrafter4500), a CMOS camera (Point Grey Chameleon3) and a computer. The resolution of the projector is 912×1140 pixels, whereas the resolution of the camera is 1280×1024 pixels. The focal length of the lens mounted on the camera is 8 mm. The projector projected the predesigned fringe patterns onto the objects, and in the meantime the camera simultaneously captured the deformed images. Afterwards, the images were sent to a computer and the 3D shape could be acquired by suitable algorithms. Figure 6 shows the experimental set-up.

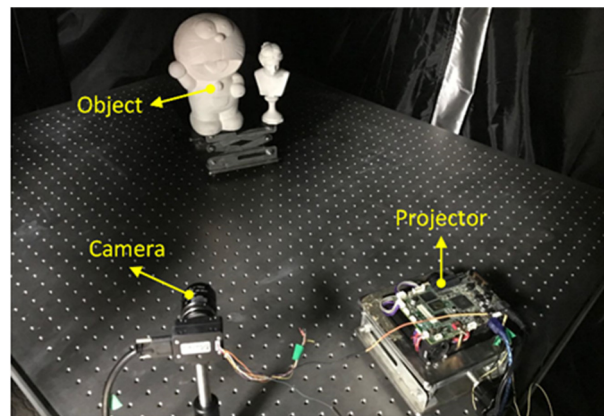


Figure 6. The experimental set-up.

4.1. Measurement of Complex Object

The first experiments tested the performance of the proposed method to measure a sculpture of Doraemon. The result is displayed in Figure 7. Figure 7a shows the captured coded pattern. Figure 7b,c present the maps of C_1 and C_2 , obtained by *Mask1* and *Mask2*, respectively. C_1 is labelled in red and C_2 is labelled in blue. In Figure 7d, the normal codewords consisting of both C_1 and C_2 are labelled in green. Obviously, there are two defective codewords on the left and right edges of Doraemon, which lost their half-code. The normal codewords can easily find their corresponding fringe orders by Table 1, whereas the fringe orders of defective codewords need to be calculated by referring to their neighbors. For example, the codeword on the right edge lost its right half-code. The left adjacent codeword is ‘31’, whose corresponding fringe order is 11. Consequently, we could acquire the fringe order of the defective codeword by 11 plus 1, and that is 12. The map of fringe orders and the result of 3D reconstruction are shown in Figure 7e,f, respectively. The 400th cross-section of two objects is presented in Figure 8. Although some codewords are defective, we can still obtain the right fringe order.

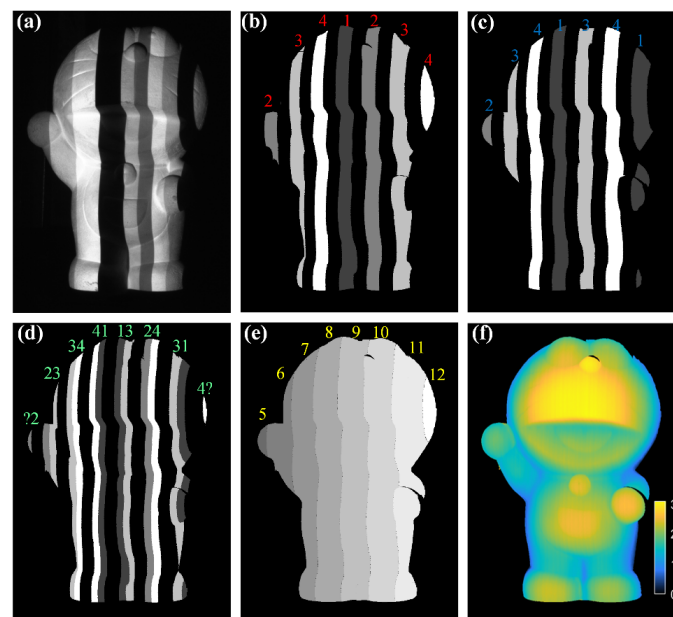


Figure 7. Processing of the sculpture of Doraemon. (a) Captured coded pattern. (b) The map of C_1 . (c) The map of C_2 . (d) The map of 2-bit codewords C_1C_2 . (e) The map of fringe orders. (f) The result of 3D reconstruction.

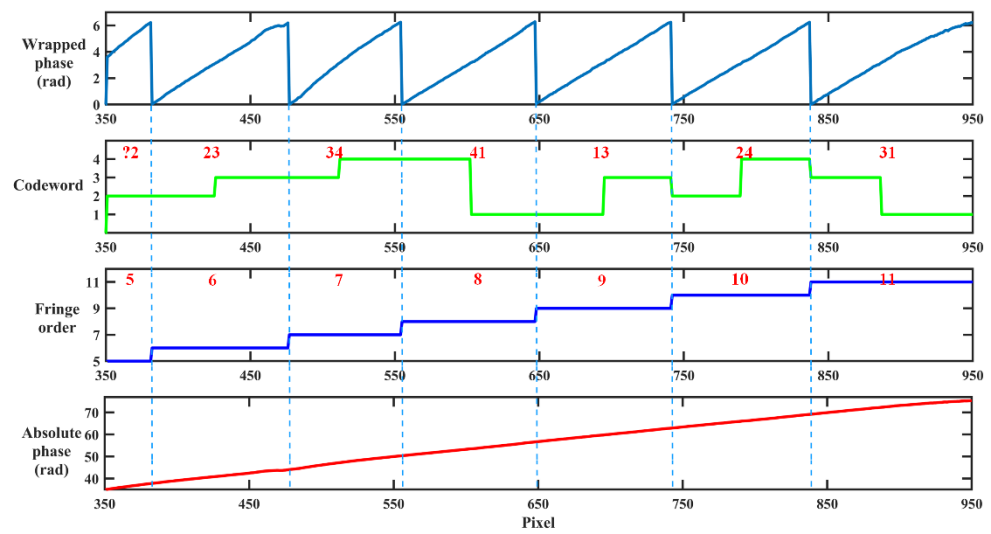


Figure 8. The 400th cross-section of two isolated sculptures.

The comparative experiments in the proposed method and the method in Ref. [32] were also set up. The results of the two methods are presented in Figure 9a,b. It can be seen that both methods can reconstruct Doraemon well and the reconstructions have a smooth surface, confirming the good performance of the proposed method when measuring a complex object.

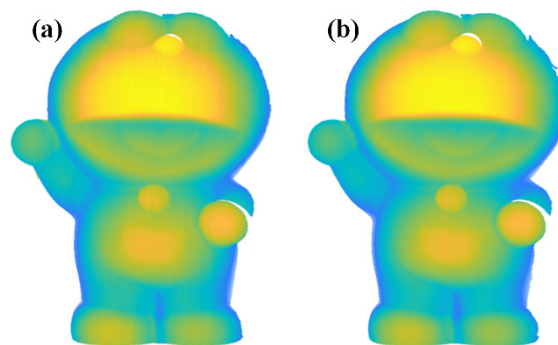


Figure 9. Three-dimensional reconstruction of the sculpture of Doraemon. (a) The proposed method. (b) Method in Ref. [32].

4.2. Measurement of the Standard Ball

The second experiment measured a standard ball to test the accuracy of the proposed method. We compared our method with Ref. [32] and the 20-step phase-shifting method. The 20-step phase-shifting method was treated as the ground truth to analyze the accuracy quantitatively. Figure 10a,b,c display the results of the 20-step phase-shifting method, the proposed method and the method in Ref. [32], respectively. It is clear that the reconstruction of the three approaches has a smooth surface. Then, the root-mean-square errors (RMSE) were computed, listed in Table 2. The two values are very close to zero and similar, indicating good accuracy of both approaches.

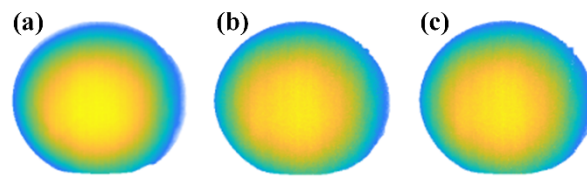


Figure 10. Three-dimensional reconstruction of the standard ball; (a) 20-step phase-shifting method. (b) The proposed method. (c) Method in Ref. [32].

Table 2. Root-mean-square errors (RMSE) between nGL and the proposed method.

Method	RMSE (rad)
The proposed method	0.0066
Ref. [32]	0.0064

4.3. Measurement under Defocused Scenes

The simulation in Section 3 demonstrates the validation of the proposed method to reconstruct objects under moderate defocused scenes. The last experiment manifests this point in real data. We take photos of the proposed method, the method in Ref. [32] and the conventional nGL method in clear scenes. Then, the pictures are slightly blurred using Equation (14) of $\sigma = 10$. Figure 11 shows the reconstruction results. Clearly, there are many white lines in the conventional nGL method, indicating inaccurate unwrapping values. On the other hand, methods of this paper and Ref. [32] could overcome the camera defocusing and obtain good results for reconstruction. Therefore, the proposed method is able to reconstruct objects in moderately defocused scenes.

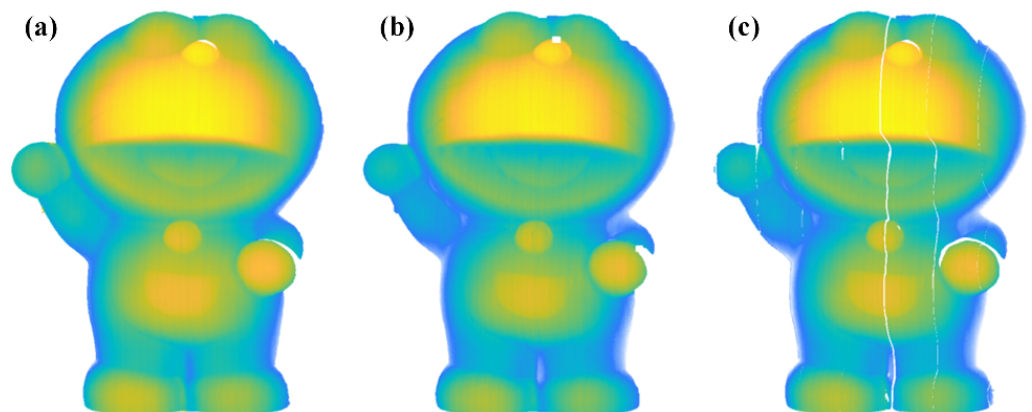


Figure 11. Three-dimensional reconstructions under defocused scenes; (a) 3D reconstruction of the proposed method; (b) 3D reconstruction of Ref. [32]; (c) 3D reconstruction of the conventional nGL method.

5. Conclusions

This paper proposes an improved gray-level method based on half-period coding, which embeds two codes in one period; thus, each period corresponds to a 2-bit codeword. The 2-bit codewords can be corrected and quantized by three masks based on the wrapped phase. Through the proposed unwrapping algorithms, fringe orders can be calculated. Various experiments demonstrate the robustness and accuracy of the proposed method. Compared with conventional gray-level methods, the proposed method only requires projection of four patterns combined with the three-step phase-shifting method, enhancing the measurement speed. In addition, this method has the ability to reconstruct objects in the defocused scene.

Author Contributions: Conceptualization, X.C.; Data curation, B.T.; Formal analysis, L.Z.; Investigation, B.T.; Methodology, Z.R.; Project administration, X.C.; Resources, X.C.; Software, Z.R.; Supervision, B.T.; Validation, Z.R.; Visualization, L.Z.; Writing—original draft, Z.R.; Writing—review and editing, X.C. All authors have read and agreed to the published version of the manuscript.

Funding: The work was supported by the National Natural Science Foundation of China (NSFC) (51905005, 51605130), Natural Science Foundation of Anhui Province (2008085QF318), Open Fund of the Key Laboratory for Metallurgical Equipment and Control Technology of Ministry of Education in Wuhan University of Science and Technology (MECOF2021B03) and Open Fund of the Key Laboratory of Icing and Anti/De-icing (Grant No. IADL20200308).

Institutional Review Board Statement: Not applicable.

Informed Consent Statement: Not applicable.

Data Availability Statement: Not applicable.

Conflicts of Interest: The authors declare no conflict of interest.

References

1. Zhong, K.; Li, Z.; Zhou, X.; Li, Y.; Shi, Y.; Wang, C. Enhanced phase measurement profilometry for industrial 3D inspection automation. *Int. J. Adv. Manuf. Technol.* **2014**, *76*, 1563–1574. [[CrossRef](#)]
2. Heist, S.; Zhang, C.; Reichwald, K.; Kuhmstedt, P.; Notni, G.; Tunnermann, A. 5D hyperspectral imaging: Fast and accurate measurement of surface shape and spectral characteristics using structured light. *Opt. Express* **2018**, *26*, 23366–23379. [[CrossRef](#)]
3. Inanç, A.; Kösoğlu, G.; Yüksel, H.; Naci İnci, M. 3-D optical profilometry at micron scale with multi-frequency fringe projection using modified fibre optic Lloyd’s mirror technique. *Opt. Lasers Eng.* **2018**, *105*, 14–26. [[CrossRef](#)]
4. Van der Jeught, S.; Dirckx, J.J.J. Real-time structured light profilometry: A review. *Opt. Lasers Eng.* **2016**, *87*, 18–31. [[CrossRef](#)]
5. Zuo, C.; Huang, L.; Zhang, M.; Chen, Q.; Asundi, A. Temporal phase unwrapping algorithms for fringe projection profilometry: A comparative review. *Opt. Lasers Eng.* **2016**, *85*, 84–103. [[CrossRef](#)]
6. Zhang, S. High-speed 3D shape measurement with structured light methods: A review. *Opt. Lasers Eng.* **2018**, *106*, 119–131. [[CrossRef](#)]
7. Zhang, S. Absolute phase retrieval methods for digital fringe projection profilometry A review. *Opt. Lasers Eng.* **2018**, *107*, 28–37. [[CrossRef](#)]
8. Xu, J.; Zhang, S. Status, challenges, and future perspectives of fringe projection profilometry. *Opt. Lasers Eng.* **2020**, *135*, 106193. [[CrossRef](#)]
9. Cai, B.; Wang, Y.; Wang, K.; Ma, M.; Chen, X. Camera Calibration Robust to Defocus Using Phase-Shifting Patterns. *Sensors* **2017**, *17*, 2361. [[CrossRef](#)]
10. Lu, P.; Sun, C.; Liu, B.; Wang, P. Accurate and robust calibration method based on pattern geometric constraints for fringe projection profilometry. *Appl. Opt.* **2017**, *56*, 784–794. [[CrossRef](#)]
11. Cai, B.; Wang, Y.; Wu, J.; Wang, M.; Li, F.; Ma, M.; Chen, X.; Wang, K. An effective method for camera calibration in defocus scene with circular gratings. *Opt. Lasers Eng.* **2019**, *114*, 44–49. [[CrossRef](#)]
12. Takeda, M.; Mutoh, K. Fourier transform profilometry for the automatic measurement of 3-D object shapes. *Appl. Opt.* **1983**, *22*, 3977. [[CrossRef](#)] [[PubMed](#)]
13. Zhang, Z.; Jing, Z.; Wang, Z.; Kuang, D. Comparison of Fourier transform, windowed Fourier transform, and wavelet transform methods for phase calculation at discontinuities in fringe projection profilometry. *Opt. Lasers Eng.* **2012**, *50*, 1152–1160. [[CrossRef](#)]
14. Kemao, Q. Applications of windowed Fourier fringe analysis in optical measurement: A review. *Opt. Lasers Eng.* **2015**, *66*, 67–73. [[CrossRef](#)]
15. Zuo, C.; Feng, S.; Huang, L.; Tao, T.; Yin, W.; Chen, Q. Phase shifting algorithms for fringe projection profilometry: A review. *Opt. Lasers Eng.* **2018**, *109*, 23–59. [[CrossRef](#)]
16. Tao, B.; Liu, Y.; Huang, L.; Chen, G.; Chen, B. 3D reconstruction based on photoelastic fringes. *Concurr. Comput. Pract. Exp.* **2021**, *34*, e6481. [[CrossRef](#)]
17. Wang, Y.; Cai, J.; Liu, Y.; Chen, X.; Wang, Y. Motion-induced error reduction for phase-shifting profilometry with phase probability equalization. *Opt. Lasers Eng.* **2022**, *156*, 107088. [[CrossRef](#)]
18. Wang, Y.; Cai, J.; Zhang, D.; Chen, X.; Wang, Y. Nonlinear Correction for Fringe Projection Profilometry With Shifted-Phase Histogram Equalization. *IEEE Trans. Instrum. Meas.* **2022**, *71*, 5005509. [[CrossRef](#)]
19. Cui, H. Reliability-guided phase-unwrapping algorithm for the measurement of discontinuous three-dimensional objects. *Opt. Eng.* **2011**, *50*, 063602. [[CrossRef](#)]
20. Zhang, S.; Li, X.; Yau, S.T. Multilevel quality-guided phase unwrapping algorithm for real-time three-dimensional shape reconstruction. *Appl. Opt.* **2007**, *46*, 50–57. [[CrossRef](#)]
21. Zhong, H.; Tang, J.; Zhang, S.; Chen, M. An Improved Quality-Guided Phase-Unwrapping Algorithm Based on Priority Queue. *IEEE Geosci. Remote Sens. Lett.* **2011**, *8*, 364–368. [[CrossRef](#)]

22. Wu, J.; Zhou, Z.; Liu, Q.; Wang, Y.; Wang, Y.; Gu, Y.; Chen, X. Two-wavelength phase-shifting method with four patterns for three-dimensional shape measurement. *Opt. Eng.* **2020**, *59*, 024107. [[CrossRef](#)]
23. Liu, K.; Wang, Y.; Lau, D.L.; Hao, Q.; Hassebrook, L.G. Dual-frequency pattern scheme for high speed 3-D shape measurement. *Opt. Express* **2010**, *18*, 5229–5244. [[CrossRef](#)] [[PubMed](#)]
24. Song, L.; Dong, X.; Xi, J.; Yu, Y.; Yang, C. A new phase unwrapping algorithm based on Three Wavelength Phase Shift Profilometry method. *Opt. Laser Technol.* **2013**, *45*, 319–329. [[CrossRef](#)]
25. Zhang, Q.; Su, X.; Xiang, L.; Sun, X. 3-D shape measurement based on complementary Gray-code light. *Opt. Lasers Eng.* **2012**, *50*, 574–579. [[CrossRef](#)]
26. Zheng, D.; Da, F.; Kema, Q.; Seah, H.S. Phase-shifting profilometry combined with Gray-code patterns projection: Unwrapping error removal by an adaptive median filter. *Opt. Express* **2017**, *25*, 4700–4713.
27. Wang, Y.; Zhang, S. Novel phase-coding method for absolute phase retrieval. *Opt. Lett.* **2012**, *37*, 2067–2069. [[CrossRef](#)]
28. Chen, X.; Wang, Y.; Wang, Y.; Ma, M.; Zeng, C. Quantized phase coding and connected region labeling for absolute phase retrieval. *Opt. Express* **2016**, *24*, 28613–28624. [[CrossRef](#)]
29. Chen, X.; Wu, J.; Fan, R.; Liu, Q.; Xiao, Y.; Wang, Y.; Wang, Y. Two-digit phase-coding strategy for fringe projection profilometry. *IEEE Trans. Instrum. Meas.* **2020**, *91*, 242–256. [[CrossRef](#)]
30. Porras-Aguilar, R.; Falaggis, K.; Ramos-Garcia, R. Optimum projection pattern generation for grey-level coded structured light illumination systems. *Opt. Lasers Eng.* **2017**, *91*, 242–256. [[CrossRef](#)]
31. Chen, X.; Chen, S.; Luo, J.; Ma, M.; Wang, Y.; Wang, Y.; Chen, L. Modified Gray-Level Coding Method for Absolute Phase Retrieval. *Sensors* **2017**, *17*, 2383. [[CrossRef](#)] [[PubMed](#)]
32. Cai, B.; Yang, Y.; Wu, J.; Wang, Y.; Wang, M.; Chen, X.; Wang, K.; Zhang, L. An improved gray-level coding method for absolute phase measurement based on half-period correction. *Opt. Lasers Eng.* **2020**, *128*, 106012. [[CrossRef](#)]
33. Ma, M.; Yao, P.; Deng, J.; Deng, H.; Zhang, J.; Zhong, X. A morphology phase unwrapping method with one code grating. *Rev. Sci. Instrum.* **2018**, *89*, 073112. [[CrossRef](#)]
34. Wang, Y.; Liu, L.; Wu, J.; Chen, X.; Wang, Y. Spatial binary coding method for stripe-wise phase unwrapping. *Appl. Opt.* **2020**, *59*, 4279–4285. [[CrossRef](#)]
35. Wu, Z.; Guo, W.; Zhang, Q. High-speed three-dimensional shape measurement based on shifting Gray-code light. *Opt. Express* **2019**, *27*, 22631–22644. [[CrossRef](#)]
36. Wu, Z.; Zuo, C.; Guo, W.; Tao, T.; Zhang, Q. High-speed three-dimensional shape measurement based on cyclic complementary Gray-code light. *Opt. Express* **2019**, *27*, 1283–1297. [[CrossRef](#)] [[PubMed](#)]
37. Tang, C.; Hou, C.; Song, Z. Defocus map estimation from a single image via spectrum contrast. *Opt. Lett.* **2013**, *38*, 1706–1708. [[CrossRef](#)] [[PubMed](#)]